

Mechanical, microstructural and mineralogical evaluation of alkali-activated waste glass and stone wool

Majda Pavlin, Barbara Horvat, Ana Frankovič, Vilma Ducman*

Slovenian National Building and Civil Engineering Institute (ZAG Ljubljana), Dimičeva 12, Ljubljana, 1000, Slovenia

ARTICLE INFO

Keywords:

Alkali-activated materials
Waste mineral wool
Curing
Mechanical properties
Microstructural evaluation

ABSTRACT

Mineral waste wool represents a significant part of construction and demolition waste (CDW) not yet being successfully re-utilized. In the present study, waste stone wool (SW) and glass wool (GW) in the form received, without removing the binder, were evaluated for their potential use in alkali activation technology. It was confirmed that both can be used in the preparation of alkali-activated materials (AAMs), whether cured at room temperature or at an elevated temperature in order to speed up the reaction. The results show that it is possible to obtain a compressive strength of over 50 MPa using SW or GW as a precursor. A strength of 53 MPa was obtained in AAM based on GW after curing for 3 days at 40 °C, while a similar compressive strength (58 MPa) was achieved after curing the GW mixture for 56 days at room temperature. In general, the mechanical properties of samples based on GW are better than those based on SW. The evolution of mechanical properties and recognition of influential parameters were determined by various microstructural analyses, including XRD, SEM, MIP, and FTIR. The type of activator (solely NaOH or a combination of NaOH and sodium silicate), and the SiO₂/Na₂O and liquid to solid (L/S) ratios were found to be the significant parameters. A lower SiO₂/Na₂O ratio and low L/S ratio significantly improve the mechanical strength of AAMs made from both types of mineral wool.

1. Introduction

Cement production significantly contributes to the global warming potential, and in 2012 it accounted for 8% of CO₂ in the environment [1]. There is a need to decrease the production of ordinary Portland cement (OPC), which has encouraged researchers to find alternatives to OPC, such as alkali-activated materials (AAMs) from waste materials. 923 million tons of construction and demolition waste (CDW; refers to concrete, bricks, gypsum, wood, glass, metal, plastic, solvents, asbestos and excavated soil) were generated by the construction industry in 2016. CDW represents 30% of all waste generated [2], and in terms of volume is the largest waste stream in the EU. By 2020, European Union legislation states that 70% CDW must be prepared for reuse, recycled or recovered [3]. Unfortunately, less than 50% of such waste is currently recycled, and the level of recycling should increase [4].

Glass and stone wool are important insulation materials for many industrial and building applications. Consequently the main source of mineral wool waste is CDW resulting from demolition. It is estimated that approximately 2,550,000 tons of mineral wool (including stone,

glass and slag wool) was produced in Europe in 2020 [3]. At the end of its lifecycle, however, it becomes a waste material which ends up in landfill. This increase high management costs and has a significant environmental impact, since mineral wool has a low density and consumes a lot of space in landfill areas, making it relatively expensive to transport. The production process, use of mineral wool products, and demolition/dismantling of buildings containing mineral wool may also release mineral wool fibres into the environment [5]. Mineral wool products produced after 1998 have a higher bio-solubility, but those produced before 1998, which are less bio-soluble, are considered as potentially carcinogenic to humans [6]. Mineral wool has been considered as carcinogenic due to its similarity to asbestos fibre [7]. However, it was found no consistent evidence connecting exposure to mineral wool with the risk of lung cancer. Mineral wool has lower bio-persistence and is removed more rapidly from the lungs than asbestos [8,9]. The deposition of inhaled fibres in the respiratory tract is a function of their physical characteristics (size, shape and density) [7]. Fibres of diameter <3.5 μm and length >5 μm with a length to diameter ratio ≥3 can be deposited in the alveolar region of the lungs [8–10].

* Corresponding author. Slovenian National Building and Civil Engineering Institute, Dimičeva 12, 1000, Ljubljana, Slovenia.

E-mail address: vilma.ducman@zag.si (V. Ducman).

URL: <http://www.zag.si> (V. Ducman).

<https://doi.org/10.1016/j.ceramint.2021.02.068>

Received 12 December 2020; Received in revised form 3 February 2021; Accepted 6 February 2021

Available online 7 February 2021

0272-8842/© 2021 The Authors. Published by Elsevier Ltd. This is an open access article under the CC BY license (<http://creativecommons.org/licenses/by/4.0/>).

Pulmonary fibrosis is caused by mineral wool fibres with low biolubility, which stay in the lungs for longer periods of time [11].

Stone and glass wool contain organic binders to hold all the fibres together, which can account for up to 5–10% of the material [9]. Phenol–formaldehyde resoles or phenol–formaldehyde–urea resins are the preferred binders used for mineral wool. Other binders, such as sodium silicates, polyesters, melamine urea formaldehyde, polyamides and furane-based resins, can also be used. They may also contain various additives, which are used to provide the final resin with the properties desired (e.g. flame retardancy, plasticization and pigmentation), or to improve processability through the use of release agents, wetting agents, and other surfactants [12].

The composition of mineral wool is similar to pozzolan materials such as fly ash, ground granulated blast-furnace slag (GGBS), and silica fume. Depending on its chemical composition and particle size, it could be used in many different applications such as to replace coarse and fine aggregates or ultra-fine fillers in concrete and cementitious materials [13]. The most commonly used approach for recycling and reusing mineral wool discussed in the literature is in the concrete industry; e.g. waste stone and glass wool could be used as supplementary cementitious materials or ultra-fine fillers [13–17], or used in fibre-reinforced cement-based mortar as a partial replacement for aggregate [18]. It has also been used for other applications, such as using stone wool fibres in hot mix asphalt to improve its dynamic properties [19], or in the development of building ceramic material, where glass wool has been reused together with lithium mine tailings from spodumene ore [20].

Due to the amorphous phase contained in waste mineral wool [21], it is a perfect material for alkali-activation. The chemical composition of stone and glass wool differs. Stone wool is composed of ~40–45 wt% SiO₂, ~16–18 wt% Al₂O₃, ~16–18 wt% CaO, and ~9–12 wt% MgO, while glass wool contains ~60–65 wt% SiO₂, ~16 wt% Na₂O, and ~7-wt.% CaO, which resembles the chemical composition of soda-lime glass [22]. Stone wool has a similar chemical composition to GGBFS, but with less CaO and MgO (~40 wt% CaO, 1.1–7.5 wt% MgO), and may form C-(N)-A-H-S gel if silicate is used as an activator [23], while in GGBFS C-S-H gel is formed, as well as C-A-S-H (at a higher aluminium content) or C-(N)-A-S-H (at a higher sodium content) [24]. Some studies have already been conducted where either stone, glass or both types of wool were used for the production of AAMs. For example, Yliniemi et al. used pure glass and stone wool for the preparation of AAMs using sodium aluminate as an alkali activator, and studied the influence of heat curing and organic resin removal on the physical and mineralogical properties of the final materials. A positive effect of organic resin on the strength of the mineral wool was observed [25]. Stone wool together with fly ash has also been applied using a sodium aluminate activator [26]. Additionally, glass wool has been used as a supplementary material in the preparation of alkali-activated iron-ore tailings [27].

Yliniemi et al. reported that an appropriate alkali activator is essential in planning the mix design of AAMs made from mineral wool. Different activators such as sodium hydroxide, sodium silicate, sodium aluminate, and sodium carbonate solution affect the kinetic reaction, setting time and compressive strength of AAMs produced using pure glass and stone wool without organic binders [22]. They also evaluated the microstructure by predicting which crystal phase and matrix gel may form in AAMs produced using stone and glass wool activated by NaOH and sodium silicate. The main reaction product formed in alkali-activated wool is an X-ray amorphous C-(N)-A-S-H-type gel in stone wool and N-A-S-H gel in glass wool [23].

In the present work, waste glass and stone wool were used as a precursor in the production of AAMs. The aim of the present research was the preparation of different AAMs based on two different types of waste mineral wool obtained from construction and demolition waste (glass and stone wool without removal of organic binder) mixed with NaOH, sodium silicate, or a combination of both activators. The effects of using two different alkali activators with various water to binder ratios on the microstructure, porosity and mechanical properties of

materials after three days of curing at 40 °C was evaluated. Using a concentrated activator may reduce the water/binder ratio necessary to provide the alkali content needed in the binder, while dilution of the alkali activator reduces its alkalinity and thus its effectiveness [28]. This work presents the results of two different SiO₂/Na₂O ratios as well as the addition of extra water to see the effect of dilution and thus different water/binder ratios on microstructures and mechanical properties. Moreover, a mixture of both types of waste mineral wool was prepared at room temperature in order to estimate the optimal mix design with respect to mechanical properties when using waste material. To date, there is no study using construction and demolition mineral wool waste with an organic binder as a precursor for alkali activation, since all research so far has been based on pure material, mostly without an organic binder.

2. Materials and methods

Two different types of mineral wool waste (glass and stone wool) were obtained from an open waste dump belonging to the quartz mining company Termit d.d. (Slovenia). Samples were first separated, shaken by hand to remove particles such as pebbles, wood and other construction materials, and then cut into small pieces. Mineral wool samples were labelled GW for glass wool and SW for stone wool, and will be referred to as such throughout the rest of the paper. The ball milling comminution method (a dry milling procedure) was chosen to mill waste material. About 1 kg of wool waste was placed in a classic concrete mixer and mixed for 2.5 h using steel balls (27 pieces, 47.5 mm in diameter). While milling and handling with the mineral wool waste, it was necessary to wear safety clothes and gloves (to cover and protect the skin against itching), safety glasses, and an FFP3 mask due to the presence of small particles (fibres) in the air. After milling, the sample was homogenized, dried in a drying oven at 105 °C for 24 h and then sieved with a 63 µm-sized mesh. The residue was again ground in the homogenizer (powder mixer shaker, Turbula T2F), using a 2L plastic container, 50 steel balls of diameter 9.8 mm, and sieved below 63 µm. The final powder material was homogenized. Different milling procedures are available to prepare powder mineral wool. None of the approaches affect the width of mineral wool fibres but they can reduce the fibre length [29].

AAMs were prepared using GW and SW sieved below 63 µm, using NaOH (Donau Chemie Ätznatron Schuppen, EINECS 215-785-5) and/or sodium silicate (12.8% Na₂O, 29.2% SiO₂, Si/Na ratio of 2.35, received from the mining company Termit) as alkali activators. For the experiments where NaOH was used as an activator, a NaOH solution with a molar concentration of 5 M was prepared. Mixtures of NaOH and sodium silicate were prepared in different proportions, by adding NaOH pellets to sodium silicate and stirring until the liquid became clear. The L/S ratio (water/binder) was manipulated by the addition of a small amount of distilled water. Following preparation the alkali activator was allowed to cool to room temperature and then poured into the sample while continuously mixing.

The milled waste material was carefully added to the alkali activator and mixed for 5 min in an overhead mixer (Tehtnica, Železniki) at 600 rpm. The paste mixtures (precursors and activators) were moulded into prisms of 80 × 20 × 20 mm³. Compressive and flexural strength was measured using a compressive and flexural strength testing machine (ToniTechnik ToniNORM) following 3 days of curing at 40 °C.

All the AAM mixtures prepared and the characteristics of the alkali activator are shown in Table 1. The mass of the precursor was the same in all sample mixtures, while the L/S ratios varied from 0.35 to 0.46 in order to ensure the prepared pastes had a suitable workability.

XRD analysis of the glass and stone wool samples was performed under cleanroom conditions in powder sample holders, using an Empyrean PANalytical X-ray Diffractometer (Cu X-Ray source, 45 kV, 40 MA, Thermo Scientific, Thermo electron SA, Ecublens, Switzerland) set between 4 and 70° at intervals of 0.0263°. Using XRD peaks

Table 1

Mix design and liquid to solid ratio (calculated according to the precursor) for AAMs developed from waste glass (GW) and stone (SW) wool.

	SW1	SW2	SW3	SW4	SW5	GW1	GW2	GW3	GW4	GW5
Mineral wool waste (g)	150	150	150	150	150	150	150	150	150	150
NaOH (g)	^a 65	3	/	/	6	^a 65	3	/	/	6
Sodium silicate (g)	/	60	120	75	120	/	60	120	75	120
Extra added H ₂ O (g)	/	20	/	20	/	/	20	/	20	/
H ₂ O _{Total} (g)	52	54.8	69.6	63.5	69.6	52	54.8	69.6	63.5	69.6
SiO ₂ /Na ₂ O (in activator)	/	1.8	2.35	2.35	1.8	/	1.8	2.35	2.35	1.8
L/S (water/binder)	0.35	0.37	0.46	0.42	0.46	0.35	0.37	0.46	0.42	0.46
pH of activator solution	>14	13.7	13.0	12.7	13.7	>14	13.7	13.0	12.7	13.7

^a NaOH of 5 M concentration was prepared.

crystallites' sizes smaller from 150 nm present in mineral wool waste and alkali-activated materials was determined using the Scherrer formula [30], and the percentage mass of amorphous phase and minerals was estimated with Rietveld refinement [31], using an external standard (a pure crystal of Al₂O₃) and X'Pert Highscore plus 4.1 software (version 4.1, Malvern Panalytical, Surrey, United Kingdom).

For XRF analysis (Thermo Scientific ARL Perform'X Sequential XRF) powder samples were first treated in a furnace for 2 h at 550 °C (Nabertherm B 150) in order to remove any organic compounds (samples were not prepared at 950 °C due to the formation of melt). Next, they were mixed with Fluxana (FX-X50-2, Lithium tetraborate 50%/Lithium metaborate 50%) in a ratio of 1:10 to lower the melting temperature. XRF analysis was performed on melted disks using the OXAS program, while data was quantified with the program UniQuant 5.

The specific surface area (BET) of the milled glass and stone wools was determined by nitrogen adsorption at 77 K over a relative pressure range of 0.05–0.3 (Micrometrics ASAP 2020, Micrometrics, Norcross, GA, USA). Before BET analysis samples were heated at 105 °C for 24 h and degassed to 0,133 Pa (Micrometrics Flowprep equipment, Micrometrics, Norcross, GA, USA).

Scanning electron microscopy (SEM; Jeol JSM-IT500) with a tungsten filament cathode as an electron source was used to investigate Au sputtered samples of the original and milled waste mineral wool samples under high vacuum. Polished alkali-activated waste mineral wool samples were prepared in epoxy resin and observed under low vacuum conditions. SEM-EDXS was performed by energy dispersive X-ray spectroscopy (EDXS; Oxford Instruments, Link Pentafet).

The pore size of the materials following alkali-activation was determined using mercury intrusion porosimetry (MIP). Small representative fragments about 1 cm³ in size (taken from a depth of approximately 1 cm), were dried for 24 h before measurement and then analysed using Micromeritics®Autopore IV 9500 equipment (Micromeritics, Norcross, GA, USA). MIP experiments were conducted on samples which had been cured at room temperature for 56 days.

Fourier-transform infrared spectroscopy (FTIR, PerkinElmer Spectrum two, Kentucky, USA), equipped with an attenuated total reflection accessory (Universal ATR) with a diamond/ZnSe crystal as a solid sample support in the range from 500 cm⁻¹–4000 cm⁻¹ with a resolution of 4 cm⁻¹ was used to evaluate the influence of different activators on the alkali-activated mineral wool samples.

Time-dependent contour plots of compressive and flexural strength were prepared with JMP 15.1.0 statistical software using the data of alkali-activated mineral wool samples cured at room temperature and 60% relative humidity. The algorithm used behind all contour plots is Delaunay triangulation of a discrete point set, in our case of the mechanical strengths and densities measured. Sample mixtures were prepared using waste stone and glass wool. All waste material contain organic binders.

3. Results and discussion

3.1. Characterization of the precursors

Data showing the chemical composition, loss of ignition (LOI) at 550 °C, specific surface area and moisture content of the different types of waste mineral wool is presented in Table 2. LOI at 550 °C is due to the removal of carbon (organic binder) and water. LOI is higher in glass wool, suggesting that GW contains a greater amount of organic binder [32]. BET analysis demonstrates similar results for both precursors, with SW having a lower specific surface area than GW. XRF analysis shows the presence of different elements in the mineral wool samples (Table 2). Mineral wools are mainly composed of silicon, aluminium, calcium, magnesium and iron (the content of oxides is stated in mass percentage). GW has a higher content of Na₂O and SiO₂ (15.0 wt% and 58.5 wt%, respectively) compared to SW (3.8 wt% Na₂O and 41.8 wt% SiO₂), but a lower amount of Al₂O₃, MgO, Fe₂O₃ and CaO (Table 2). During the collection of waste material, however, it is difficult to completely separate GW and SW, meaning the final material (i.e. GW) may have traces of SW and vice versa.

SEM pictures before (a and b) and after (c and d) grinding the GW and SW are presented in Fig. 1. Samples are composed of different fibres which vary in size and diameter, consisting of cylindrical rods and irregular randomly-shaped particles. Although all material was put through a 63 µm sieve, some particles larger than 63 µm remain. Some particles with a diameter smaller than 63 µm may enter perpendicularly through the mesh during the sieving process (Fig. 1c and d). SW involves many so-called “shoots” (rounded particles) as a consequence of its production process [7]. It is easier to sieve SW compared to GW which could be attributed to the higher content of organic binder in the GW waste (Table 2).

3.2. Microstructural and mineralogical analysis of alkali-activated material

3.2.1. SEM analysis

Backscattered electron (BSE) micrographs of polished alkali-

Table 2

Chemical composition and loss of ignition (LOI) at 550 °C determined by the gravimetric method, BET analysis and moisture content for both glass and stone wool.

Chemical component (%)	Glass wool [GW]	Stone wool [SW]
Na ₂ O	15.0	3.82
SiO ₂	58.5	41.8
Al ₂ O ₃	4.06	15.1
MgO	5.24	11.0
Fe ₂ O ₃	0.90	5.11
CaO	8.95	16.0
Other oxides	1.55	2.55
Total	94.2	95.4
LOI 550 °C (%)	5.80	4.62
BET (m ² /g)	0.6331	0.3848
Moisture content (wt. %)	0.57	0.17

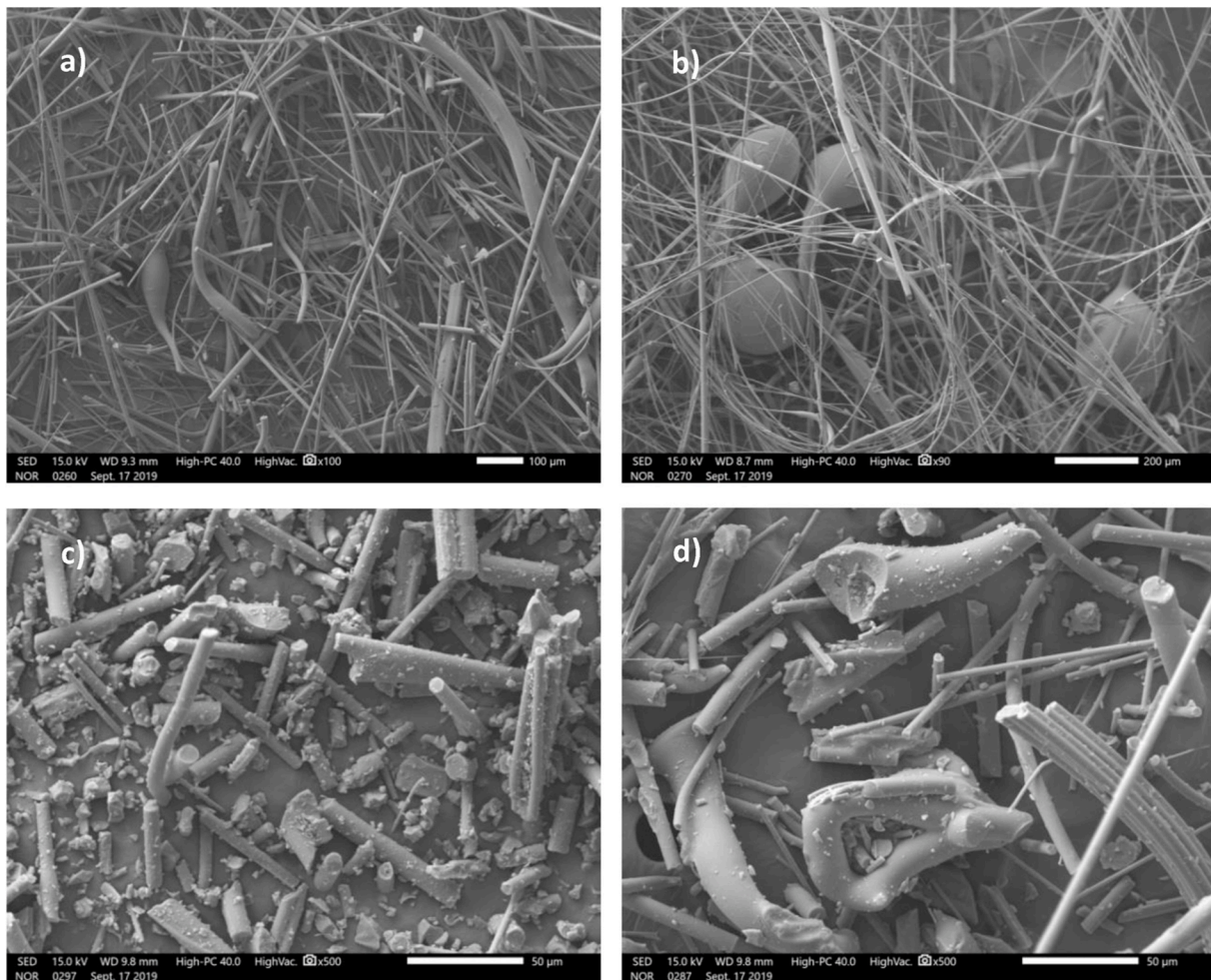


Fig. 1. SEM pictures of GW (a) and SW (b) before pulverizing. After grinding, samples were sieved below 63 μm . Figure c) represents glass wool with different elongated particles, while in figure d) many randomly-shaped particles next to the stone wool fibres are visible.

activated GW and SW are presented in Fig. 2. The micrographs show that unreacted fibres remain present in the samples following alkali-activation. This indicates incomplete dissolution, and the amount of unreacted fibres is dependent on the type of alkali activator used in the alkali activation process. All micrographs show uniformly distributed and randomly oriented fibres in the binder matrix. Alkali-activation with NaOH results in many unreacted particles (fibres) in both SW1 and GW1 samples. The matrices in SW1 and GW1 differ, showing a porous structure (Fig. 2). Precursors (GW, SW) activated with sodium silicate formed a denser and more homogenous matrix than when activated with only NaOH. The differences between GW and SW are seen in Fig. 2. GW samples include microcracks in the structure while SW samples have a more porous structure without any microcracks. GW2 has a lower L/S ratio and shows fewer microcracks while a less porous structure is observed in SW2 and SW4 compared to the other SW samples. Micro-cracks, which were primarily observed in the GW samples, might indicate a loss of water during hardening, sample pre-treatment, and/or when exposed to the low-vacuum conditions of SEM [23]. Also, in SW samples, some “shoots” are observed as bigger particles with a more rounded shape.

3.2.2. SEM-EDXS analysis

Mix designs for all the prepared mixtures (GW1–GW5 and SW1–SW5) are shown in Table 1.

The L/S ratio slightly differed between mix designs, ranging between 0.35 and 0.46. Mix designs of GW and SW labelled with the same

number (1–5) have the same L/S ratio. GW and SW have different chemical compositions, which affects the L/S ratio and the amount of Na, Ca, Si and Al in the AAM, as shown by the different molar ratios of Si/Na, Si/Al and Ca/Si given in Table 3. Data were calculated using XRF and XRD data or EDXS data. XRF and XRD data gave the average distribution of elements in the system, while data obtained by EDXS considered point analysis of the gel matrix to evaluate the dissolution of elements during alkali activation and the formation of any gel potentially present in each AAM sample. When high amounts of Na and Si and a low amount of Al is present in the system (i.e. glass wool), the Si/Na molar ratio decreases and the Si/Al ratio increases. Since different mix designs were applied, it was not possible to prepare all samples with the same L/S ratio while maintaining equal workability.

According to the literature, the optimal Si/Al and Na/Al ratios are 1.9 and 1 respectively, due to the charge balancing nature of the negatively-charged tetrahedral aluminium centers [33]. The most appropriate ratios for Si/Al and Si/Na are, however, hard to achieve for mineral wool waste samples, due to variations in chemical composition, the amount of amorphous phase, and the behavior of particle-fibres. XRF and XRD data revealed a noticeable difference between the Si/Al ratios of the SW and GW samples. EDXS data showed an elevated Si/Al ratio in all samples, especially in the GW AAMs. The Si/Al ratio was lower when the material was activated with NaOH, meaning no extra silicon was introduced into the system, and the Si present in the gel is a consequence of Si dissolution. The Si/Na ratio obtained by EDXS is lower in SW1, possibly due to incorporation of Na in the gel matrix, while the ratio of

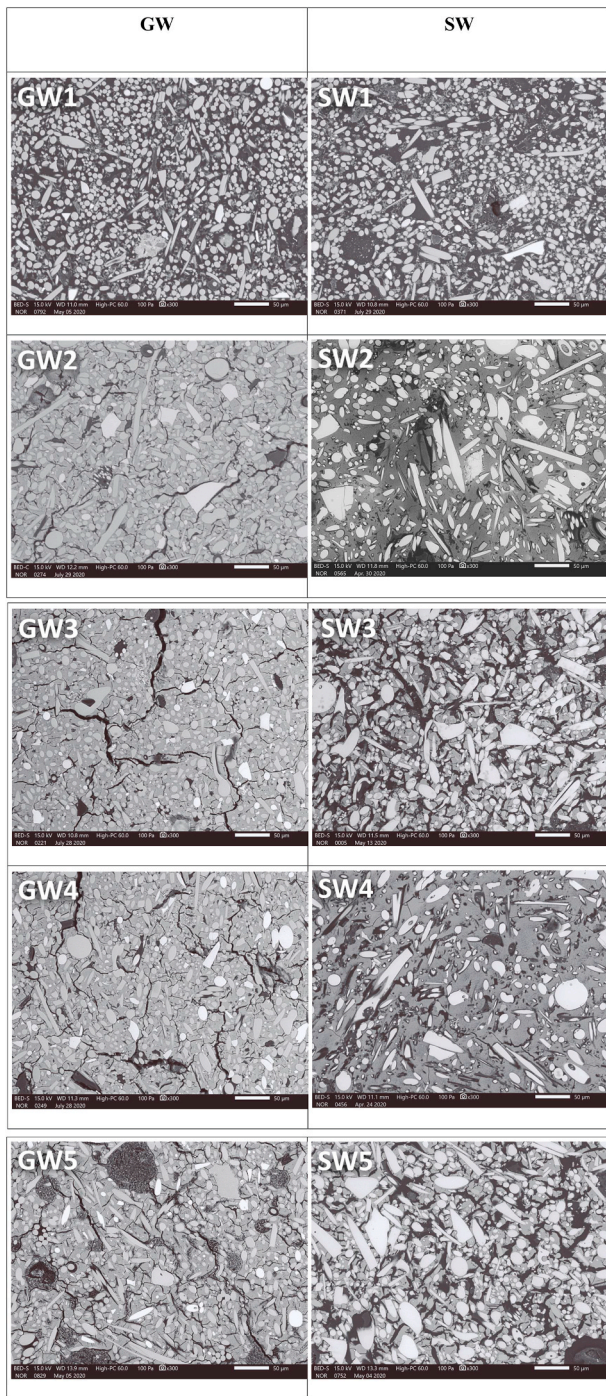


Fig. 2. SEM-BSE micrographs of alkali-activated materials (GW, SW) after 3 days of curing at 40 °C.

Table 3

Molar ratios between the different elements involved in alkali activation (values calculated according to XRD and XRF data or obtained by SEM-EDXS). The data obtained by XRF and XRD are normalized to aluminium.

Ratio	SW	SW1	SW2	SW3	SW4	SW5	GW	GW1	GW2	GW3	GW4	GW5
Si/Al (XRD and XRF)	2.32	2.33	2.98	3.62	3.10	3.62	12.1	12.1	14.5	17.0	15.1	16.8
Si/Na (XRD and XRF)	5.59	2.14	2.62	2.37	2.77	1.94	1.99	1.42	1.66	1.66	1.74	1.47
Ca/Si (XRD and XRF)	0.40	0.41	0.32	0.25	0.31	0.25	0.15	0.16	0.12	0.11	0.13	0.12
Si/Al (EDXS)	/	2.76	4.65	6.95	5.01	3.77	/	18.6	25.2	32.7	33.4	29.4
Si/Na (EDXS)	/	1.55	2.23	2.70	2.43	2.20	/	1.40	2.76	3.22	3.08	1.67
Ca/Si (EDXS)	/	0.36	0.31	0.18	0.22	0.31	/	0.18	0.19	0.17	0.20	0.09

Si/Na in the GW1 sample is the same as from data obtained by XRF and XRD. The Ca/Si ratio is higher in SW1 samples compared to GW1. GW, however, contains more Si and less Ca, and dissolution of Ca and Si is favored, as seen by the increased Ca/Si and Si/Al ratios shown in Table 4.

Alkali-activation with sodium silicate increases the Si/Al ratio, particularly in the GW samples. Providing extra silicate in the mixture by adding sodium silicate led to the formation of sodium silicate gel with greater connectivity. An increase in the Si/Al ratio was also observed in the SW samples. EDXS results for AAMs activated with sodium silicate show Ca/Si ratio values between 0.09 and 0.20 for GW samples and 0.18–0.31 for SW samples. It is known that the higher alkalinity in GGBFS reduces the dissolution of Ca but increases the solubility of Si and Al [34–36]. The higher mechanical strength of GGBFS obtained when it was activated with sodium silicate compared to NaOH was explained by the consumption of Ca^{2+} , which dissolves during alkali activation and reacts with silicate species, forming dense C-A-S-H reaction products [37]. The chemical composition of SW is closer to GGBFS than GW, and the Ca/Si ratio shown in Table 3 indicates higher values for the SW samples. C-A-S-H gel is also expected in GGBFS activated with NaOH in a higher proportion because no extra Si has been added into the system. In this study, the Ca/Si ratio was slightly higher when samples were activated with NaOH compared to those activated with sodium silicate. Due to the increased Na content in the gel matrix, the formation of C-(N)-A-S-H and N-A-S-H gel would be possible, as observed in the study by Yliniemi et al. [23]. In AAMs using GGBFS the Ca/Si ratio was between 0.6 and 0.7 when activated by sodium silicate, compared to 0.9–1.0 in the case of NaOH. Due to the lower Ca content in SW samples, however, the ratios in this study are lower and C-(N)-A-S-H and N-A-S-H gels are more likely present [38]. Where GW samples were activated using sodium silicate it is suggested that Ca was incorporated into the N-A-S-H gel, as is typical for low calcium precursors. Partial substitution of Ca in N-(A)-S-H gel, as a consequence of Ca dilution at a higher alkalinity, is possible [23]. Additional studies are needed to evaluate the possibility of different gel phases present in the GW and SW systems.

3.2.3. XRD analysis

XRD analyses of the precursors and their alkali-activated counterparts are shown in Fig. 3 X-ray diffraction patterns of the precursors (GW and SW) and alkali-activated materials (GW1–GW5 and SW1–SW5). AAMs were cured at 40 °C for 3 days. The halo, typical of an amorphous fraction, shifted towards higher 2θ values after alkali activation (this is more evident in the case of GW than in SW). The mineral content of samples before and after alkali-activation, as determined by XRD, is presented in Fig. 3, alongside crystallite size determined by the Scherrer equation [39] and data regarding the goodness of fit. The goodness of fit is between 5.47 and 7.99, which is more than ideal (an ideal value is 1), because waste material was evaluated avoiding false-positive results, which could give a lower GOF, but the results would not even fit XRF data. The minerals common to both types of precursor are quartz, dolomite and calcite, while, according to Rietveld refinement, more than 97% of the material is amorphous (pt). Most of the SiO_2 detected in the initial materials by XRF was therefore amorphous and readily available for reaction. Following alkali-activation of GW and SW more than 97% of amorphous phase still remains in the hardened material. Similar to

Table 4

Percentage (pt – mass percentage) of minerals and amorphous phase in GW and SW and their alkali-activated counterparts according to Rietveld refinement, and size of crystallite domains calculated by the Scherrer equation (S).

Mohs hardness scale [M]	Quartz (ICSD 98-016-2490)		Calcite (ICSD 98-003-7241)		Thermonatrite (ICSD 98-000-1852)		Dolomite (ICSD 98-018-5049)		Amorphous phase (%)	Goodness of fit
	7	3	1–1.5	3.5–4						
GW	pt [%]	0.9	1.0	/		1.0	97.0	6.32		
	S [nm]	65	60	/		60				
SW	pt [%]	0.5	0.7	/		1.1	97.7	5.63		
	S [nm]	65	50	/		60				
GW1	pt [%]	0.5	/	1.0		0.5	98.0	6.21		
	S [nm]	90	/	70		55				
GW2	pt [%]	0.8	0.9	/		1.1	97.2	7.47		
	S [nm]	60	50	/		50				
GW3	pt [%]	0.8	0.8	/		1.1	97.3	7.94		
	S [nm]	50	50	/		50				
GW4	pt [%]	1.2	0.8	/		1.1	96.9	7.51		
	S [nm]	90	50	/		50				
GW5	pt [%]	1.5	/	/		1.0	97.5	7.99		
	S [nm]	100	/	/		50				
SW1	pt [%]	0.3	0.6	1.0		/	98.1	5.53		
	S [nm]	70	50	60		/				
SW2	pt [%]	0.3	/	/		/	99.7	6.37		
	S [nm]	150	/	/		/				
SW3	pt [%]	0.7	0.8	/		1.1	97.4	6.84		
	S [nm]	60	50	/		50				
SW4	pt [%]	1.4	/	/		0.7	97.9	6.47		
	S [nm]	100	/	/		50				
SW5	pt [%]	0.6	0.8	/		1.1	97.3	7.02		
	S [nm]	60	50	/		50				

pt [%] = percentage of the crystalline phase; S [nm] = crystalline size according to Scherer equation.

the precursors, the AAMs contain quartz, dolomite and calcite. When NaOH was used as an alkali activator, thermonatrite was present in the samples due to excess sodium in the mixture.

3.3. Mechanical properties of the alkali-activated materials

3.3.1. Mechanical properties after curing at 40 °C for 3 days

The waste mineral GW and SW samples were alkali-activated using NaOH, sodium silicate or a combination of the two. The effect of the L/S ratio on microstructure and mechanical strength was studied. Results detailing the compressive and flexural strength of the various AAMs are presented in Fig. 4 and Table S1 in the supplement. After 3 days curing at 40 °C, compressive strength was higher in the mixtures prepared with GW compared to those made from SW. Nevertheless, the sample strength is dependent on the L/S ratio and the type of activator used. When using only NaOH (GW1, SW1), the compressive strength was approximately 15 MPa for GW and 25 MPa for SW after 3 days curing at 40 °C. The better compressive strength observed in the case of SW might be attributed to the faster hardening compared to GW. SW contains a higher proportion of calcium, and the dissolution of calcium may affect its early strength since calcium enables faster setting [22]. As seen by the SEM pictures in Fig. 2, the SW1 sample has a denser microstructure than GW1, as it contains more calcium. Using an NaOH molarity of 6.25 M, Yliniemi et al. found compressive strength to be 20 MPa after one day of curing at 40 °C, similar to our findings using 5 M NaOH, where a compressive strength of 25 MPa was obtained following 3 days of curing at 40 °C (L/S ratio was the same in both studies). Using 5 M NaOH for the

alkali activation of GW, we achieved a compressive strength of more than 5 MPa, greater than a sample cured for only one day [22]. In the present work, all samples were cured at 40 °C for 3 days, and, since elevated temperature accelerate the reaction process and thus hardening of materials, the compressive strength of GW1 is therefore higher than in the study of Yliniemi et al.. Although the extent of reaction is greater when NaOH is used as an activator, less binder gel is formed because, unlike in the case of sodium silicate, no external Si is available for polymerization. The drying process differs from that with sodium silicate, which alters the formation of pores and consequently weakens the binder.

Using sodium silicate as an activator (GW3, SW3), or a combination of both activators (NaOH and sodium silicate in GW5 and SW5), significantly improves the compressive strength (Fig. 4), giving values above 27 and 31 MPa for SW3 and SW5, respectively, and approximately 38 MPa for GW samples (GW3 and GW5). Since the L/S ratio is the same in both cases, the addition of NaOH leads to an improvement in the SW5 sample but not in the GW5. The lowest L/S ratio in the GW2 and SW2 mixtures resulted in a significantly improved compressive strength compared to the SW5 and GW5 samples, with the strength of the SW samples increasing from 31 MPa to 40 MPa and the GW samples from 38 MPa to 53 MPa. The molar ratios of SiO₂/Na₂O (in activator) were the same in all AAMs prepared (SW2, GW2, SW5, GW5). A lower amount of sodium silicate was used in the SW2 and GW2 samples, so the L/S ratio is the lowest. The workability of the prepared paste was, however, good enough to prepare AAMs, due to the extra water added to the sodium silicate. The addition of water in sodium silicate slightly decreases the

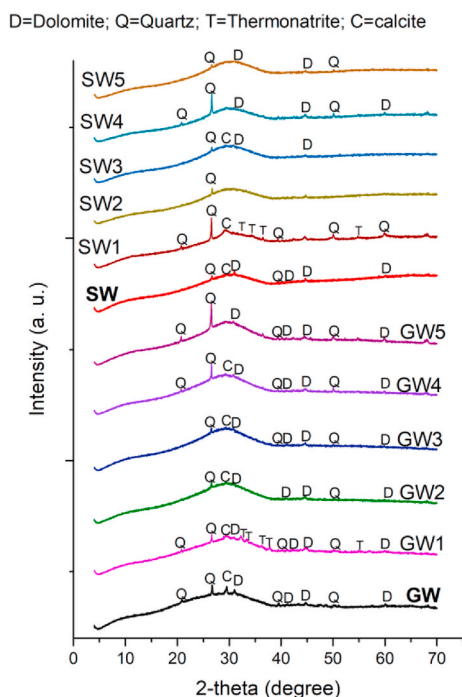


Fig. 3. X-ray diffraction patterns of the precursors (GW and SW) and alkali-activated materials (GW1-GW5 and SW1-SW5). AAMs were cured at 40 °C for 3 days.

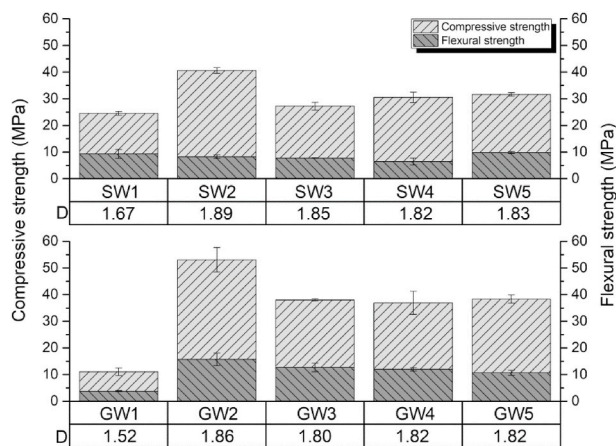


Fig. 4. Compressive strength, flexural strength and density (D; kg dm⁻³) for the various alkali-activated glass (GW) and stone (SW) wool samples after 3 days curing at 40 °C.

compressive strength of GW4 compared to GW3, resulting in a value of around 37 MPa. The standard deviation of measurements for the GW4 samples is greater than in the case of the GW3 samples, however. The SW3 and SW4 samples show the opposite trend, with a slight increase in compressive strength in the SW4 sample. The L/S ratio in the SW4 and GW4 samples is, however, lower than that in SW3 and GW3.

The flexural strength was below 10 MPa in the SW mixtures tested and exhibited a similar flexural strength across all mixtures (SW1 9.3, SW2 8.3, SW3 7.5 and SW5 9.8 MPa), except in GW4, where the flexural strength was slightly lower at 6.5 MPa. The flexural strength was above 10 MPa in all the GW-based AAMs (GW2 15.7, GW3 12.7, GW4 12.0 and GW5 10.7 MPa), except in the mixture activated by NaOH (GW1, 3.8 MPa). It follows that all GW samples prepared show an increase in flexural strength if either sodium silicate or a mix of both activators were used simultaneously. The addition of water in the GW4 and SW4

samples decreases the flexural strength compared to the GW3 and SW3 samples, which had no added water, despite the fact that the L/S ratio was lower in sample mixture 4 than in sample mixture 3. This indicates the importance of the higher amount of silicon added in sample mixture 3 compared to mixture 4. Similar to compressive strength, the GW2 sample has the highest flexural strength amongst all GW and SW samples. This trend was not observed in the SW2 sample.

The density of the various mixtures is shown in Fig. 4. The density of the AAMs depends on the type of alkali activator used. The nominal densities of all samples are higher when using sodium silicate compared to when using NaOH. With NaOH, the densities are 1.52 for GW1 and 1.67 kg dm⁻³ for SW1. These two samples have lower compressive strengths than other samples, especially GW1 (Fig. 4), but the flexural strength of the SW1 sample is the highest among SW samples. The higher density and mechanical strengths in the SW1 sample compared to the GW1 sample could be due to the higher degree of reaction and formation of a denser structure, as seen in Fig. 2. Higher amounts of unreacted material increase the defect density in the specimens and have a deleterious effect on the mechanical strength of the AAMs [33]. Both samples have many unreacted particle-fibres (Fig. 2); however, the gel formed between the fibres in SW1 improves the mechanical strength. The density increased to more than 1.80 kg dm⁻³ in the AAMs made using either sodium silicate or a combination of both alkali activators (a mixture of NaOH and sodium silicate). The GW2 and SW2 samples have the highest densities, consistent with the lowest L/S.

3.3.2. Mechanical properties after curing at room temperature

In the next step, curing at room temperature was studied using GW5 and SW5. The compressive and flexural strengths were measured after curing for 1, 3, 7, 14, 28, 56 and 90 days at room temperature. The results are shown in Fig. 5 and Table S2 in the supplement. After 3 days of curing at room temperature, samples were still too soft to be demoulded. After one week, the compressive strengths for SW5 and GW5 were 9.6 and 6.1 MPa, respectively. Curing at room temperature for 28 days (Fig. 5) resulted in similar compressive strengths for both types of wool, with a value of 34.1 MPa in the case of stone wool (SW5) and 32.2 MPa (GW5) in glass wool. When samples were cured for 3 days at 40 °C (Fig. 4), the compressive strength of glass wool (38.4 MPa) was better than that of stone wool (31.6 MPa). The flexural strength after 7 days at room temperature ranged between 2 and 3 MPa in both types of AAM. After 28 days of curing, the flexural strength increased to 9.6 in GW5 and 8.7 MPa in SW5. After curing the AAMs for 3 days at 40 °C the flexural strength was 10.7 in GW5 and 9.8 MPa in SW5. These differences indicate that neither curing at 40 °C for 3 days nor 28 days at room

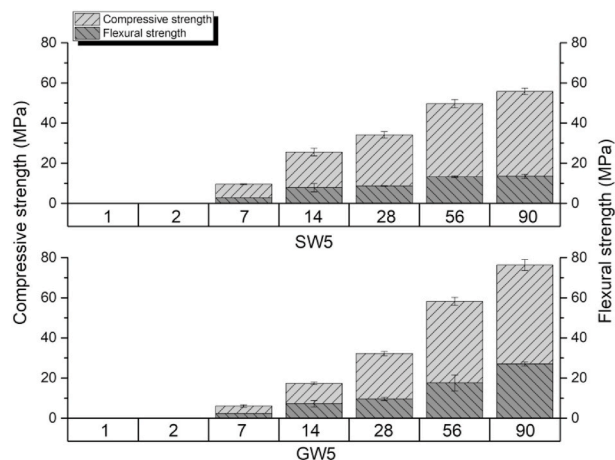


Fig. 5. The compressive and flexural strength of alkali-activated GW5 and SW5 samples measured after curing at room temperature for 1, 3, 7, 14, 28, 56 and 90 days.

temperature is sufficient to develop the final compressive or flexural strength of the AAMs. Fig. 5 clearly shows the compressive and flexural strengths of GW5 nearly double after 56 days. A higher mechanical strength is also observed in the SW5 sample. Increases in the compressive and flexural strength were observed after 90 days in both AAMs, however, with SW5 showing an improvement in compressive strength of about 6 MPa and GW5 increasing by almost 20 MPa to approximately 76 MPa. Similarly, a significant increase was observed in the flexural strength of the GW5 sample after 90 days curing at room temperature, while almost no difference was seen in SW5 (Fig. 5). Improvements in mechanical strength occur because of the increase in Si–O–Si bonds, which result from the activation with sodium silicate and dissolution of silicon from the GW precursor.

A model of time-dependent compressive and flexural strength is shown in Fig. 6. Contour plots include the data for GW5 up to 90 days of curing at room temperature, where compressive strength reached almost 80 MPa and flexural strength approximately 27 MPa, and after 90 days for SW5, which achieved compressive and flexural strengths of approximately 56 MPa and 13 MPa respectively. A mixture of different proportions of GW and SW was included in the contour plots in order to evaluate the most suitable mix design. Compressive strength is highest when the proportion of GW is more than 75%. The contour plots indicate far better flexural strength when a mixture of both types of wool was used. It follows that a mixture of the two types of wool improves the mechanical properties earlier compared to the use of pure waste material (labelled as 0 and 1 in the graph). If the mixture contained more than 50% GW, the compressive strengths were higher after 50 days, while the highest values of flexural strength after 50 days were observed when the mix design contained 75% GW. A higher proportion of glass wool improves the mechanical properties, while using a mixture of both types of wool accelerated the reaction, probably due to the presence and dissolution of more Ca from SW, which decreases the setting time. The increased compressive strength in samples based on GW or mixtures containing GW may be attributed to a higher Si/Al ratio and thus a higher number of Si–O–Si bonds [40] compared to the SW mix designs.

3.4. Porosity determined by mercury intrusion porosimetry (MIP)

Porosity values of the alkali-activated GW and SW samples, measured by MIP, are presented in Table 5, alongside data regarding compressive strength, L/S ratios and the proportion of gel and capillary pores. Pore size distribution was between 0.01 and 100 μm , and the total porosities of samples cured at 40 °C for 3 days are presented in Fig. 7.

Porosity values are shown as the percentage of total volume. Total porosity ranged between 25 and 32% in the alkali-activated SW samples and between 15 and 34% in the GW samples. Porosity for the GW samples (GW2–GW5) was generally lower than in the SW samples, with the exception of GW1. The lower porosity in the GW samples (GW2–GW5) is consistent with the higher mechanical strength in these samples. The GW2 sample, which had the highest compressive and flexural strength, does not, however, have the lowest porosity. Samples with the highest porosity were prepared using waste mineral wool and sodium hydroxide, while the mixtures prepared with sodium silicate or a combination of both activators have a lower porosity. Comparisons between SW1, GW1 and SW2, GW2 samples, with L/S ratios of 0.35 and 0.37 respectively (Table 5), reveal that the GW2/SW2 have far better mechanical properties and a lower porosity. Using sodium silicate as the activator not only led to higher strengths but also to a lower-porosity binder [33,41,42].

The total porosity was lower in samples where only sodium silicate was used as an activator (GW3, GW4), compared to those with the addition of NaOH (GW2, GW5). The lowest total porosity was in sample GW3, at 15.2%, followed by sample GW4 with a value of 16.3%, where a small amount of water had been added to the sodium silicate to improve workability. If the total porosity decreases, the pore size distribution curve shifts to smaller pore sizes, indicating a denser microstructure of the samples (Fig. 2). The reduced porosity and refined microstructure is attributed to a higher degree of reaction in the samples. A higher reaction degree of the precursor leads to more reaction products, filling the pore space and consequently resulting in a denser microstructure [43]. The initial pores in the alkali-activated samples may, however, form during preparation (mixing), when the paste is gravity-cast in the moulds, and/or in the early stages of the curing process, when pores and micro-cracks can form due to drying shrinkage [44]. Additional pores might form during alkali-activation due to the presence of organic binder in the SW and GW waste samples. The alkali activator reacts with the organic material where the self-foaming effect was observed. An example of an AAM sample with a porous structure in the presence of organic binder is shown in Fig. S1 in the supplement. Self-foaming has been observed previously when using other types of waste as a precursor [45].

According to the literature, a peak with a pore diameter between 0.01 and 0.1 μm corresponds to the pore diameter of the gel pore system, and a pore size larger than 0.1 μm represents the capillary pore system [43]. In the present work, the largest proportion of pores in the samples have a pore size of 0.1–1, 1–2 and 2–10 μm . Pore size distribution differs

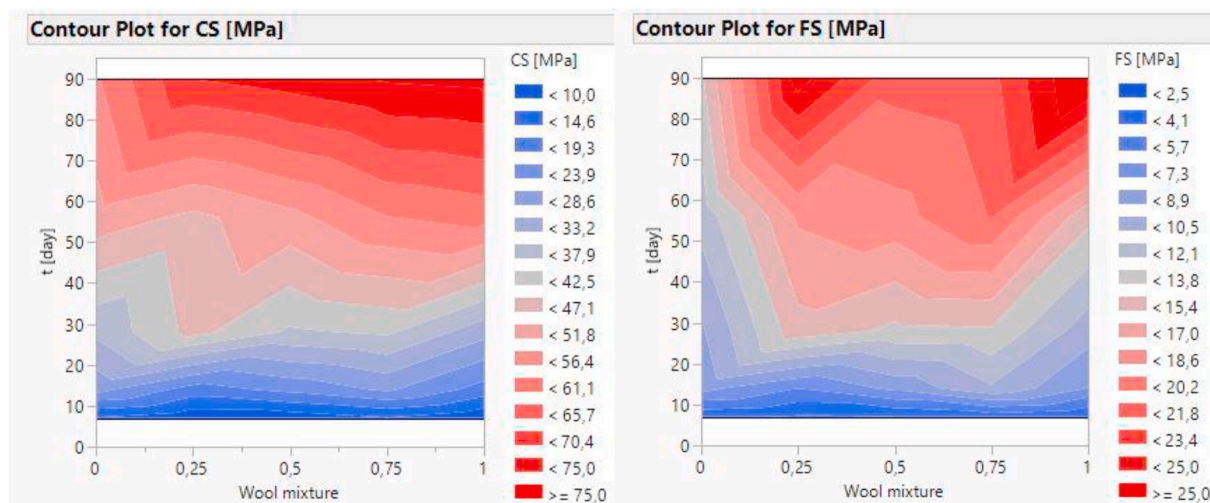
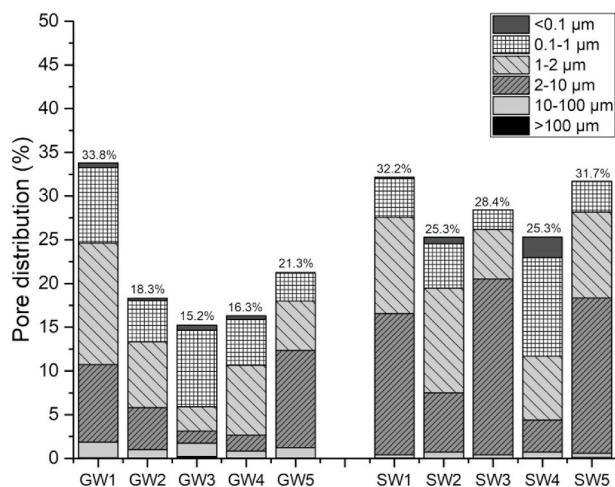


Fig. 6. Model prediction of time-dependent flexural and compressive strength in glass wool (1), stone wool (0) and a mixture of the two types of wool (between 0 and 1). The sum of both wools is 1, where 0 represents 100% SW and 1 represents 100% GW. The distance between contour lines for the compressive and flexural strengths represents the speed of solidification of the mix.

Table 5

Sample data showing average pore diameter, porosity, percentage of gel and capillary pores, water/binder ratio (L/S) and compressive strength.

	SW1	SW2	SW3	SW4	SW5	GW1	GW2	GW3	GW4	GW5
Average Pore Diameter (4 V/A)	1.31	0.18	1.81	0.47	1.73	1.11	0.31	0.14	0.13	1.64
Porosity	32.2	25.3	28.4	25.3	31.7	33.8	18.3	15.2	16.3	21.3
Apparent (skeletal) density	2.41	2.45	2.46	2.21	2.41	2.29	2.29	2.24	2.23	2.30
0.01–0.1 μm (%)	0.16	0.74	0	2.34	0.01	0.55	0.30	0.6	0.59	0.03
0.1–100 μm (%)	99.3	96.9	99.9	90.6	99.7	98.1	98.1	94.7	96.9	99.6
L/S	0.35	0.37	0.46	0.42	0.46	0.35	0.37	0.46	0.42	0.46
Compressive strength (MPa)	24.5	40.6	27.2	30.6	31.6	15.2	53.1	38	36.9	38.4

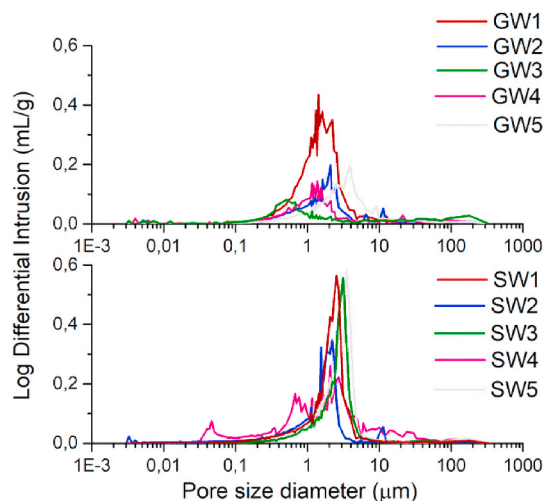
**Fig. 7.** Pore size distribution in the GW and SW samples. Samples were cured at 40 °C for 3 days.

between the GW and SW samples. The GW samples show a similar pattern of pore size distribution, ranging from 2 to 10 μm and decreasing when only sodium silicate was used. The GW2, GW3 and GW4 samples, with a lower total porosity, have a reduced proportion of pore size 2–10 μm . A lower proportion of pore size 2–10 μm was observed in the SW2 and SW4 samples compared to the SW1, SW3 and SW5 samples with a higher porosity. The L/S ratios are lower in SW2 and SW4 compared to the other samples, and they show a higher proportion of pores sized 0.1–1. These two samples also contain pores <0.1 μm , which are not present or are present only in a small proportion in other samples. The microstructures of the SW2 and SW4 samples show the formation of a different matrix compared to samples SW1, SW3 and SW5 (Fig. 2). A lower porosity, and the formation of smaller pores, is consistent with the SEM micrographs, which show less unreacted stone wool fibres in SW2 and SW4 compared to the other three samples (Fig. 2).

Fig. 8 represents the graph of pore size distribution versus the logarithms of differential intrusion curves, as derived from MIP. The GW and SW samples show a unimodal distribution ranging between 0.01 and 10 μm . GW5 has a maximum height of 3.9 μm compared to values of 1.6 and 2.2 μm for GW1 and GW2, respectively. The highest peak among the GW mixtures is in GW1, indicating the highest porosity in this sample, while in the case of stone wool SW1, SW3 and SW5 all show comparable peak heights at similar positions. SW2 and SW4 show a wider pore size distribution. The addition of extra water in the SW mixtures may induce the formation of different, smaller pores.

3.5. FTIR analysis

Fig. 9 represents the FTIR spectra of precursors (GW, SW) and their associated AAMs. Each spectrum of the initial mineral wool waste shows one wide band, representing the Si–O–T (T = Si or Al) asymmetric stretching vibration band, which occurs at 905 cm^{-1} in SW and 945 cm^{-1} in GW. In both cases, the broad bands indicate a disordered silicate

**Fig. 8.** Pore size distribution of GW and SW samples cured for 3 days at 40 °C.

structure. The lower positioned band seen in the SW indicates that the vitreous phase has more Al–O and Al–O–Si bonds compared to the GW sample, which is consistent with the chemical composition of the SW precursor. During the dissolution step, Al–O–Si and Al–O–Al bands are broken more readily than the Si–O–Si bands, which results in weaker bonds between network-forming and network-modifying species [46, 47]. This corresponds to the higher reactivity of the SW precursor to alkali attack in comparison to the GW samples, which was evidenced by faster hardening and an increase in mechanical strength in the first days of curing at room temperature, as shown in Fig. 6.

During the alkali activation of SW and GW, the band representing asymmetric stretching of T–O–T (T = Si or Al) shifted to higher wavenumbers (between 953 cm^{-1} and 979 cm^{-1}), indicating polymerization of the Si–O network [48]. A narrowing of the peak was observed in all AAMs, due to the more condensed tetrahedral species [37]. Shifts in the SW and GW samples depend on the exact position of the Si/Al ratio. Increasing the content of the tetrahedrally positioned Al in the system and substituting Si^{4+} for Al^{3+} reduces the T–O–T angle, which results in the band shifting to lower wavenumbers due to a smaller bonding force [49]. GW and SW differ in their chemical composition and, accordingly, their Si/Al ratios also differ (Table 3). The Si/Al ratio is above 5 for all the GW mix designs (EDXS data in Table 3), where it is suggested that aluminium is incorporated in the stable cyclic and larger aluminosilicate species whereas when the Si/Al ratio is smaller than 5, the bulk of all aluminium is present as monomeric $\text{Al}(\text{OH})_4^-$ [50]. Since the Si/Al ratio is much lower in SW than in GW, and that shifts are similar regardless of which wool was used, parameters other than the Si/Al ratio may influence the position of the peak.

The extent of the shift depends on the type of precursor, the reaction time and the curing conditions [51]. The shifts depend on the activator used, with sodium silicate causing a shift to higher values (967–979 cm^{-1}) compared to the use of NaOH alone (954–960 cm^{-1}). Higher alkalinity decreases the wavenumber due to the lower extent of

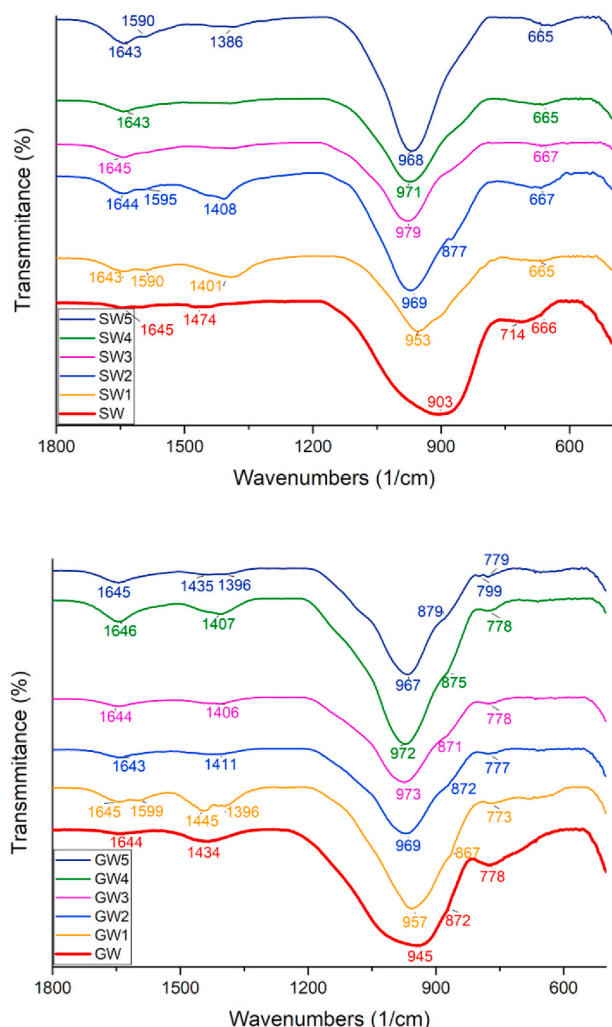


Fig. 9. FTIR spectra of the precursors and alkali-activated wool waste mixtures cured at 40 °C for 3 days.

polymerization in the matrix [52] and a decrease in network connectivity [53]. This is seen from the SEM pictures (Fig. 2) when NaOH was used as the alkali activator, where many unreacted fibres remain present in the matrix. Moreover, the pH of NaOH is higher compared to other samples (Table 1), and the position of SW1 and GW1 at lower wavenumbers are therefore consistent with the pH values. Furthermore, small differences were also observed between the mixtures where only sodium silicate or a combination of both activators was used. In AAMs where NaOH was added to sodium silicate solution the band is positioned at slightly lower wavenumbers (SW2, SW5, GW2, GW5) compared to the samples which used sodium silicate only. This indicates a similar degree of polymerization, although the alkalinity of the activator shifts the position of these bands to lower values compared to SW3, SW4, GW3 and GW4.

In general, shifts in all the mix designs were similar, regardless of which wool waste was used, given that the precursors (SW and GW) contained a sufficient amount amorphous Si. The GW precursor, however, contained more Si, as determined by XRF, and analysis of the dissolution of glass wool in NaOH shows a higher concentration of Si in GW compared to SW [54]. The shift of T–O–T (T = Si or Al) occurs at lower wavenumbers in SW1 samples than in GW1 samples, which agrees with the previous statement. It follows that, due to similar shifts in all mix designs, the soluble silicate in the sodium alkaline activator significantly contributes to the formation of the framework of the gel phase in the binders [55].

A band ranging between 770 and 780 cm^{-1} which indicates a Si–O band (in the SiO_4 tetrahedron), is present in all the GW samples [56]. This band was not observed in the SW samples. In the SW samples, as well as in the SW precursor, a band was observed at approximately 666 cm^{-1} , which was attributed to symmetrical stretching of Si–O–T [38]. A transmission band at approximately 1645 cm^{-1} indicates the presence of H–O–H bending vibration, due to the presence of water in the AAM or waste adsorbed at the surface of the GW precursor. Some AAM samples show bands ranging between 1400 and 1500 cm^{-1} , which correspond to the asymmetric stretching of CO_3^{2-} (O–C–O), and a weak shoulder at around $\sim 870 \text{ cm}^{-1}$ due to out-of-plane bending of CO_3^{2-} . It is not, however, possible to prevent the incorporation of CO_2 if the sample is exposed to air [48]. These bands are more pronounced in the GW samples. A higher Ca/Si ratio may indicate more intensive bands, as observed in the SW1 and SW2 samples, where, according to EDXS analysis (Table 3), the Ca/Si ratio is the highest in the matrix.

4. Conclusion

The performance of AAMs depends on the waste mineral wool used. The key findings are as follows:

- the results confirm that both precursors are suitable for the alkali activation process,
- successful mechanical properties were obtained following both curing regimes (curing either at 40 °C or at room temperature), achieving a compressive strength of over 50 MPa in both cases,
- the compressive strength after 3 days curing at 40 °C was better in GW than in SW if sodium silicate or a combination of sodium silicate and NaOH were used,
- L/S affects the final mechanical properties regardless of which wool was used,
- A lower $\text{SiO}_2/\text{Na}_2\text{O}$ ratio and low L/S ratio significantly improve the mechanical strength of both materials,
- Contour plots of pure waste GW, SW and a mixture of the two, showed the highest mechanical properties when the mixture contained 75% of GW,
- XRD analysis of precursors and samples following alkali activation confirmed more than 97% amorphous phase,
- SEM pictures show the differing microstructures of AAMs prepared from SW or GW. These differences result from the chemical composition of the precursors themselves, as well as the alkali activator used. Differences in the porosity are also noticed, with SW-based materials having a more porous structure.
- Many unreacted fibres are present in alkali-activate materials made from both types of wool waste. The partial dissolution of GW and SW fibres shows the formation of different binder gels, as expected due to the different chemical compositions of the precursors, and point identification made by SEM-EDXS.

This study confirms the potential for the secondary use of mineral wool waste as a precursor in the development of alkali-activated construction materials. In order to enable the transfer of this technology into praxis, further investigations will be performed to find a suitable additive to either accelerate the reaction or increase early strength at room temperature. Due to the huge amount of waste wool available, its use as a raw material for various applications would be an important step toward a circular economy.

Declaration of competing interest

The authors declare that they have no known competing financial interests or personal relationships that could have appeared to influence the work reported in this paper.

Acknowledgements

H2020 project Wool2Loop has received funding from the European Union's Horizon 2020 research and innovation programme under grant agreement No. 821000. The opinions expressed in this document only reflect the authors' view and in no way reflect the European Commission's opinions. The European Commission is not responsible for any use that may be made of the information it contains.

The study was also supported by the project No. C3330-17-529032 Raziskovalci-2.0-ZAG-529032" granted by the Ministry of Education, Science and Sport of the Republic of Slovenia. The investment is co-financed by the Republic of Slovenia, Ministry of Education, Science and Sport and the European Regional Development Fund.

The Metrology Institute of the Republic of Slovenia is acknowledged for the use of XRF.

Appendix A. Supplementary data

Supplementary data to this article can be found online at <https://doi.org/10.1016/j.ceramint.2021.02.068>.

References

- J.G.I. Olivier, J.A.H.W. Peters, G. Janssens-Maenhout, *Trends in Global CO₂ Emissions 2012 Report*, 2012.
- M. Migliore, C. Talamo, G. Paganin, in: M. Migliore, C. Talamo, G. Paganin (Eds.), *Construction and Demolition Waste BT - Strategies for Circular Economy and Cross-Sectoral Exchanges for Sustainable Building Products: Preventing and Recycling Waste*, Springer International Publishing, Cham, 2020, pp. 45–76, https://doi.org/10.1007/978-3-030-30318-1_2.
- O. Väntsi, T. Kärki, Mineral wool waste in Europe: a review of mineral wool waste quantity, quality, and current recycling methods, *J. Mater. Cycles Waste Manag.* 16 (2014) 62–72, <https://doi.org/10.1007/s10163-013-0170-5>.
- P. Villoria Sáez, M. del Río Merino, C. Porras-Amores, Estimation of construction and demolition waste volume generation in new residential buildings in Spain, *Waste Manag. Res.* 30 (2011) 137–146, <https://doi.org/10.1177/0734242X11423955>.
- T. Sattler, R. Pomberger, J. Schimek, D. Vollprecht, *MINERAL WOOL WASTE IN AUSTRIA, ASSOCIATED HEALTH ASPECTS AND RECYCLING OPTIONS*, 2020, p. 174. Detritus.
- E.C. Regulation, No. 1272/2008 of the European Parliament and of the Council of 16 December 2008 on classification, labelling and packaging of substances and mixtures, amending and repealing Directives 67/548/EEC and 1999/45/EC, and amending Regulation (EC) No 1907/2006, EC, Amend. Regul. (E. Luxemb. Off. J. Eur. Union 31 (December 2008) (2008) L353.
- E. Nielsen, P. Nørhede, O. Ladefoged, L. Tobiassen, Evaluation of Health Hazards by Exposure to Mineral Wools (Glass, Stone/slag, HT) and Proposal of a Health-Based Quality Criterion for Ambient Air, 2013. <https://www2.mst.dk/Udgiv/publications/2013/12/978-87-93026-68-1.pdf>.
- I.W.G. on the E. of C.R. to Humans, I.A. for R. on Cancer, *Man-made Mineral Fibres and Radon*, World Health Organization, 1988.
- I.W.G. on the E. of C.R. to Humans, I.A. for R. on Cancer, *W.H. Organization, Man-made Vitreous Fibres*, World Health Organization, 2002.
- W.H.O. (World H. Organization), *Man-made mineral fibres, Environ. Health Criter.* 77 (1988).
- M. Williams, P.R. McClure, *Toxicological Profile for Synthetic Vitreous Fibers*, 2004.
- S. Kowatsch, in: L. Pilato (Ed.), *Mineral Wool Insulation Binders BT - Phenolic Resins: A Century of Progress*, Springer Berlin Heidelberg, Berlin, Heidelberg, 2010, pp. 209–242, https://doi.org/10.1007/978-3-642-04714-5_10.
- A. Cheng, W.-T. Lin, R. Huang, Application of rock wool waste in cement-based composites, *Mater. Des.* 32 (2011) 636–642, <https://doi.org/10.1016/J.MATDES.2010.08.014>.
- L. Wei-Ting, C. An, H. Ran, W. Yuan-Chieh, H. Ta-Yuan, Rock wool wastes as a supplementary cementitious material replacement in cement-based composites, *Comput. Concr.* 11 (2013) 93–104, <https://doi.org/10.12989/CAC.2013.11.2.093>.
- K.D.C. Silva, G.C. Silva, J.F. Natali, J.C. Mendes, G.J.B. Silva, R.A.F. Peixoto, Rock wool waste as supplementary cementitious material for Portland cement-based composites, *ACI Mater. J.* 115 (2018) 653–661, <https://doi.org/10.14359/51701100>.
- K.C.S. Defaveri, J.C. Mendes, J.M.F. de Carvalho, W.C. Fontes, R.A.F. Peixoto, G.J. S. Brigolini, Glass wool residue: a potential supplementary cementitious material, *ACI Mater. J.* 116 (2018) 43–49, <https://doi.org/10.14359/51716679>.
- W.-T. Lin, A. Cheng, R. Huang, S.-Y. Zou, Improved microstructure of cement-based composites through the addition of rock wool particles, *Mater. Char.* 84 (2013) 1–9, <https://doi.org/10.1016/J.MATCHAR.2013.06.020>.
- C. Piña Ramírez, E. Atanes Sánchez, M. del Río Merino, C. Viñas Arrebola, A. Vidales Barriguete, Feasibility of the use of mineral wool fibres recovered from CDW for the reinforcement of conglomerates by study of their porosity, *Construct. Build. Mater.* 191 (2018) 460–468, <https://doi.org/10.1016/j.conbuildmat.2018.10.026>.
- H. Behbahani, V. Najafi Moghaddam Gilani, R. Salehfarid, D. Safari, Evaluation of fatigue and rutting behaviour of hot mix asphalt containing rock wool, *Int. J. Civ. Eng.* 18 (2020) 1293–1300, <https://doi.org/10.1007/s40999-020-00532-5>.
- P.N. Lemougna, J. Yliniemi, H. Nguyen, E. Adesanya, P. Tanskanen, P. Kinnunen, J. Roning, M. Illikainen, Utilisation of glass wool waste and mine tailings in high performance building ceramics, *J. Build. Eng.* 31 (2020) 101383, <https://doi.org/10.1016/j.jobte.2020.101383>.
- J.M. Cáceres, J. Hernández, J.M. Rincón, Characterization of fibers as rockwool for insulation obtained from canary islands basalts, *Mater. Construcción* 46 (1996) 61–78.
- J. Yliniemi, B. Walkley, J.L. Provis, P. Kinnunen, M. Illikainen, Influence of activator type on reaction kinetics, setting time, and compressive strength of alkali-activated mineral wools, *J. Therm. Anal. Calorim.* (2020), <https://doi.org/10.1007/s10973-020-09651-6>.
- J. Yliniemi, B. Walkley, J.L. Provis, P. Kinnunen, M. Illikainen, Nanostructural evolution of alkali-activated mineral wools, *Cement Concr. Compos.* 106 (2020) 103472, <https://doi.org/10.1016/j.cemconcomp.2019.103472>.
- J. Provis, J. Deventer, *Alkali Activated Materials: State-Of-The-Art Report*, RILEM TC 224-AAAM, 2014, <https://doi.org/10.1007/978-94-007-7672-2>.
- J. Yliniemi, P. Kinnunen, P. Karinkanta, M. Illikainen, Utilization of mineral wools as alkali-activated material precursor, *Materials* 9 (2016) 312, <https://doi.org/10.3390/ma9050312>.
- P. Kinnunen, J. Yliniemi, B. Talling, M. Illikainen, Rockwool waste in fly ash geopolymer composites, *J. Mater. Cycles Waste Manag.* (2016), <https://doi.org/10.1007/s10163-016-0514-z> full text available at: <http://rdcu.be/negh>.
- K. do Carmo e Silva Defaveri, L.F. dos Santos, J.M. Franco de Carvalho, R.A. F. Peixoto, G.J. Brigolini, Iron ore tailing-based geopolymer containing glass wool residue: a study of mechanical and microstructural properties, *Construct. Build. Mater.* 220 (2019) 375–385, <https://doi.org/10.1016/j.conbuildmat.2019.05.181>.
- J.W. Phair, J.S.J. Van Deventer, Effect of the silicate activator pH on the microstructural characteristics of waste-based geopolymers, *Int. J. Miner. Process.* 66 (2002) 121–143, [https://doi.org/10.1016/S0301-7516\(02\)00013-3](https://doi.org/10.1016/S0301-7516(02)00013-3).
- J. Yliniemi, O. Laitinen, P. Kinnunen, M. Illikainen, Pulverization of fibrous mineral wool waste, *J. Mater. Cycles Waste Manag.* (2017), <https://doi.org/10.1007/s10163-017-0692-3>.
- B. Ingham, M.F. Toney, X-ray diffraction for characterizing metallic films, *Met. Film. Electron. Opt. Magn. Appl.* (2014) 3–38, <https://doi.org/10.1533/9780857096296.1.3>.
- H. Rietveld, A profile refinement method for nuclear and magnetic structures, *J. Appl. Crystallogr.* 2 (1969) 65–71, <https://doi.org/10.1107/S0021889869006558>.
- O. Heiri, A. Lotter, G. Lemcke, Loss on ignition as a method for estimating organic and carbonate content in sediments: reproducibility and comparability of results, *J. Paleolimnol.* 25 (2001), <https://doi.org/10.1023/A:1008119611481>.
- P. Duxson, J.L. Provis, G.C. Lukey, S.W. Mallicoat, W.M. Kriven, J.S.J. van Deventer, Understanding the relationship between geopolymer composition, microstructure and mechanical properties, *Colloid. Surf. A Phys. Eng. Asp.* 269 (2005) 47–58, <https://doi.org/10.1016/J.COLSURFA.2005.06.060>.
- C. Shi, R.L. Day, Selectivity of alkaline activators for the activation of slags, *Cem. Concr. Aggregates* 18 (1996) 8–14.
- A. Fernández-Jiménez, F. Puertas, Effect of activator mix on the hydration and strength behaviour of alkali-activated slag cements, *Adv. Cement Res.* 15 (2003) 129–136, <https://doi.org/10.1680/acr.2003.15.3.129>.
- S. Song, D. Sohn, H.M. Jennings, T.O. Mason, Hydration of alkali-activated ground granulated blast furnace slag, *J. Mater. Sci.* 35 (2000) 249–257, <https://doi.org/10.1023/A:1004742027117>.
- A. Fernández-Jiménez, F. Puertas, I. Sobrados, J. Sanz, Structure of calcium silicate hydrates formed in alkaline-activated slag: influence of the type of alkaline activator, *J. Am. Ceram. Soc.* 86 (2003) 1389–1394, <https://doi.org/10.1111/j.1151-2916.2003.tb03481.x>.
- B. Walkley, R. San Nicolas, M.-A. Sani, J.D. Gehman, J.S.J. van Deventer, J. L. Provis, Phase evolution of Na₂O–Al₂O₃–SiO₂–H₂O gels in synthetic aluminosilicate binders, *Dalton Trans.* 45 (2016) 5521–5535, <https://doi.org/10.1039/C5DT04878H>.
- P. Scherrer, *Bestimmung der Größe und der inneren Struktur von Kolloidteilchen mittels Röntgenstrahlen*, *Nachrichten von Der Gesellschaft Der Wissenschaften, Göttingen. Math. Klasse.* 2 (1918) 98–100.
- P. Duxson, S. Mallicoat, G.C. Lukey, W.M. Kriven, J.S.J. van Deventer, Microstructural characterisation of metakaolin-based geopolymers, *Adv. Ceram. Matrix Compos. X.* (2006) 71–85, <https://doi.org/10.1002/9781118408353.ch7>.
- M. Criado, A. Fernández-Jiménez, A.G. de la Torre, M.A.G. Aranda, A. Palomo, An XRD study of the effect of the SiO₂/Na₂O ratio on the alkali activation of fly ash, *Cement Concr. Res.* 37 (2007) 671–679, <https://doi.org/10.1016/j.cemconres.2007.01.013>.
- R.R. Lloyd, J.L. Provis, K.J. Smeaton, J.S.J. van Deventer, Spatial distribution of pores in fly ash-based inorganic polymer gels visualised by Wood's metal intrusion, *Microporous Mesoporous Mater.* 126 (2009) 32–39, <https://doi.org/10.1016/j.micromeso.2009.05.016>.
- Y. Zuo, G. Ye, Pore structure characterization of sodium hydroxide activated slag using mercury intrusion porosimetry, nitrogen adsorption, and image analysis, *Mater. (Basel, Switzerland)* 11 (2018) 1035, <https://doi.org/10.3390/ma11061035>.
- Y. Ma, G. Ye, The shrinkage of alkali activated fly ash, *Cement Concr. Res.* 68 (2015) 75–82, <https://doi.org/10.1016/j.cemconres.2014.10.024>.

- [45] B. Horvat, V. Ducman, Influence of particle size on compressive strength of alkali activated refractory materials, *Materials* 13 (2020) 2227.
- [46] B.H.W.S. de Jong, G.E. Brown, Polymerization of silicate and aluminate tetrahedra in glasses, melts and aqueous solutions—II. The network modifying effects of Mg^{2+} , K^+ , Na^+ , Li^+ , H^+ , OH^- , F^- , Cl^- , H_2O , CO_2 and H_3O^+ on silicate polymers, *Geochem. Cosmochim. Acta* 44 (1980) 1627–1642, [https://doi.org/10.1016/0016-7037\(80\)90216-1](https://doi.org/10.1016/0016-7037(80)90216-1).
- [47] Y. Xiao, A.C. Lasaga, Ab initio quantum mechanical studies of the kinetics and mechanisms of silicate dissolution: H^+ (H_3O^+) catalysis, *Geochem. Cosmochim. Acta* 58 (1994) 5379–5400, [https://doi.org/10.1016/0016-7037\(94\)90237-2](https://doi.org/10.1016/0016-7037(94)90237-2).
- [48] P. Yu, R.J. Kirkpatrick, B. Poe, P.F. McMillan, X. Cong, Structure of calcium silicate hydrate (C-S-H): near-, mid-, and far-infrared spectroscopy, *J. Am. Ceram. Soc.* 82 (1999) 742–748, <https://doi.org/10.1111/j.1151-2916.1999.tb01826.x>.
- [49] A. Fernández-Jiménez, A. Palomo, Mid-infrared spectroscopic studies of alkali-activated fly ash structure, *Microporous Mesoporous Mater.* 86 (2005) 207–214, <https://doi.org/10.1016/j.micromeso.2005.05.057>.
- [50] N. Azizi, R.K. Harris, A. Samadi-Maybodi, Aluminium-27 NMR investigation of the influence of cation type on aluminosilicate solutions, *Magn. Reson. Chem.* 40 (2002) 635–639, <https://doi.org/10.1002/mrc.1071>.
- [51] O. Rudić, V. Ducman, M. Malešev, V. Radonjanin, S. Draganić, S. Šupić, M. Radeka, Aggregates obtained by alkali activation of fly ash: the effect of granulation, pelletization methods and curing regimes, *Materials* 12 (2019) 776, <https://doi.org/10.3390/ma12050776>.
- [52] S.A. Bernal, J.L. Provis, V. Rose, R. Mejía de Gutierrez, Evolution of binder structure in sodium silicate-activated slag-metakaolin blends, *Cement Concr. Compos.* 33 (2011) 46–54, <https://doi.org/10.1016/j.cemconcomp.2010.09.004>.
- [53] C.A. Rees, J.L. Provis, G.C. Lukey, J.S.J. van Deventer, In situ ATR-FTIR study of the early stages of fly ash geopolymer gel formation, *Langmuir* 23 (2007) 9076–9082, <https://doi.org/10.1021/la701185g>.
- [54] K. König, K. Traven, M. Pavlin, V. Ducman, Evaluation of locally available amorphous waste materials as a source for alternative alkali activators, *Ceram. Int.* (2020), <https://doi.org/10.1016/j.ceramint.2020.10.059>.
- [55] R.R. Lloyd, J.L. Provis, J.S.J. van Deventer, Microscopy and microanalysis of inorganic polymer cements. 2: the gel binder, *J. Mater. Sci.* 44 (2009) 620–631, <https://doi.org/10.1007/s10853-008-3078-z>.
- [56] M. Torres-Carrasco, A. Palomo, F. Puertas, *Sodium Silicate Solutions from Dissolution of Glass Wastes, Statistical analysis*, 2014.